

Electronic band structure in pristine and Sulfur-doped Ta₂NiSe₅

Tanusree Saha,^{1,*} Luca Petaccia,² Barbara Ressel,¹ Primož Rebernik Ribič,² Giovanni Di Santo,² Wenjuan Zhao,² and Giovanni De Ninno^{1,2}

¹Laboratory of Quantum Optics, University of Nova Gorica, 5001 Nova Gorica, Slovenia

²Elettra Sincrotrone Trieste, Strada Statale 14 km 163.5, 34149 Trieste, Italy

(Dated: June 1, 2022)

We present an angle-resolved photoemission study of the electronic band structure of the excitonic insulator Ta₂NiSe₅, as well as its evolution upon Sulfur doping. Our experimental data show that while the excitonic insulating phase is still preserved at a Sulfur-doping level of 25%, such phase is heavily suppressed when there is a substantial amount, $\sim 50\%$, of S-doping at liquid nitrogen temperatures. Moreover, our photon energy-dependent measurements reveal a clear three dimensionality of the electronic structure, both in Ta₂NiSe₅ and Ta₂Ni(Se_{1-x}S_x)₅ ($x = 0.25, 0.50$) compounds. This suggests a reduction of electrical and thermal conductivities, which might make these compounds less suitable for electronic transport applications.

I. INTRODUCTION

The dimensionality and degree of anisotropy in electronic transport and optical properties of layered materials, such as, MoS₂^{1,2}, ReS₂³ and other transition-metal dichalcogenides⁴, make them potentially suitable for the fabrication of new electronic and optoelectronic devices. A recent addition to the family of such materials are the ternary chalcogenides, Ta₂NiX₅ ($X \rightarrow \text{Se/S}$), which have attracted attention due to their layered crystalline structure and in-plane anisotropic properties⁵⁻⁷. In both materials, the transition metal atoms and the chalcogen atoms are arranged forming a chain pattern in each layer and the layers are stacked by van der Waals forces⁸. While the ground state of Ta₂NiSe₅ is an excitonic insulator (EI)⁹⁻¹¹, Ta₂NiS₅ does not show any evidence of hosting an excitonic insulating phase and is a normal semiconductor in its ground state¹². An excitonic insulator state is realised in materials where the valence and conduction bands are separated by a very small energy gap ($E_g > 0$) or there is a small overlap in energies of the band edges ($E_g < 0$). The attractive Coulomb force between electrons and holes in a narrow gap semiconductor or in a semimetal lead to the formation of bound electron-hole pairs, known as excitons¹³⁻¹⁶. The formation of excitons in a system gives rise to an intriguing ground state, namely, the excitonic insulator¹⁷, which is characterised by a larger band gap that mirrors the exciton binding energy E_b .

The pre-requisite for the spontaneous formation of excitons is $|E_b| > |E_g|$ and the excitonic state will be most stable in a zero band gap material ($E_g = 0$). Since E_g is usually significantly larger than E_b in semiconductors and insulators, materials with nearly zero energy gap or nearly zero energy overlap ($E_g \approx 0$ such that a small E_b can establish the EI ground state) are chosen as potential candidates in the search of excitonic insulators. The spontaneous formation of excitons is suppressed with increasing values of $|E_g|$, i.e., for more positive values of E_g when $E_g > 0$ (in a semiconductor) and for more negative values of E_g when $E_g < 0$ (in a semimetal), leading to a decrease in the values of the EI transition

temperature T_c . As $|E_g|$ is increased such that it is comparable to or larger than the exciton binding energy, i.e., when $|E_g| \gtrsim E_b$, the excitonic phase becomes increasingly unstable against the semiconducting/semimetallic ground state^{14,16}. The energy gap E_g can be controlled through chemical substitution or by applying physical pressure^{18,19}.

The EI phase has been identified in a number of materials, such as TiSe₂^{20,21}, Ta₂NiSe₅¹⁹, TmSe_{1-x}Te_x²², InAs/GaSb quantum wells²³, etc. However, the phase transition in some of these materials is strongly influenced by lattice and spin degrees of freedom^{24,25}, for example, a charge density wave (CDW) or a band Jahn-Teller effect put forward for 1T-TiSe₂^{26,27}. In this respect, Ta₂NiSe₅ has emerged as a promising candidate for hosting a canonical excitonic insulator phase, excluding any alternative scenarios such as lattice distortion-mediated CDW mechanism leading to the phase transformation. However, Ta₂NiSe₅ also undergoes an orthorhombic to monoclinic structural phase transition^{8,28} in addition to EI transition which raises a question on the dominant origin of the order parameter in this material. This triggered numerous experimental and theoretical²⁹⁻³¹ studies that used either equilibrium^{10,32-34} or non-equilibrium^{35,36} approaches trying to resolve the issue. The question on the dominant origin of the order parameter in Ta₂NiSe₅ has also been addressed in one of our recent works³⁷. The scope of this paper is not to identify the origin of the phase transition but to investigate the effect of increasing E_g on the electronic band structure of Ta₂NiSe₅ and the dimensionality in pure and doped compounds. The increase of E_g is obtained by introducing Sulfur atoms at Selenium sites. Beyond a certain doping limit, x , the excitonic insulating phase in Ta₂Ni(Se_{1-x}S_x)₅ is completely suppressed¹⁹, a signature of which is the absence of a second-order phase transition in resistivity measurements. As x increases, changes in hybridization between Ni and Se/S valence band orbitals lead to a monotonic increase of the bandgap E_g and, as consequence to a reduction of T_c . Application of physical pressure also results in the reduction of T_c in pristine Ta₂NiSe₅¹⁹.

Angle-resolved photoemission spectroscopy is an ex-

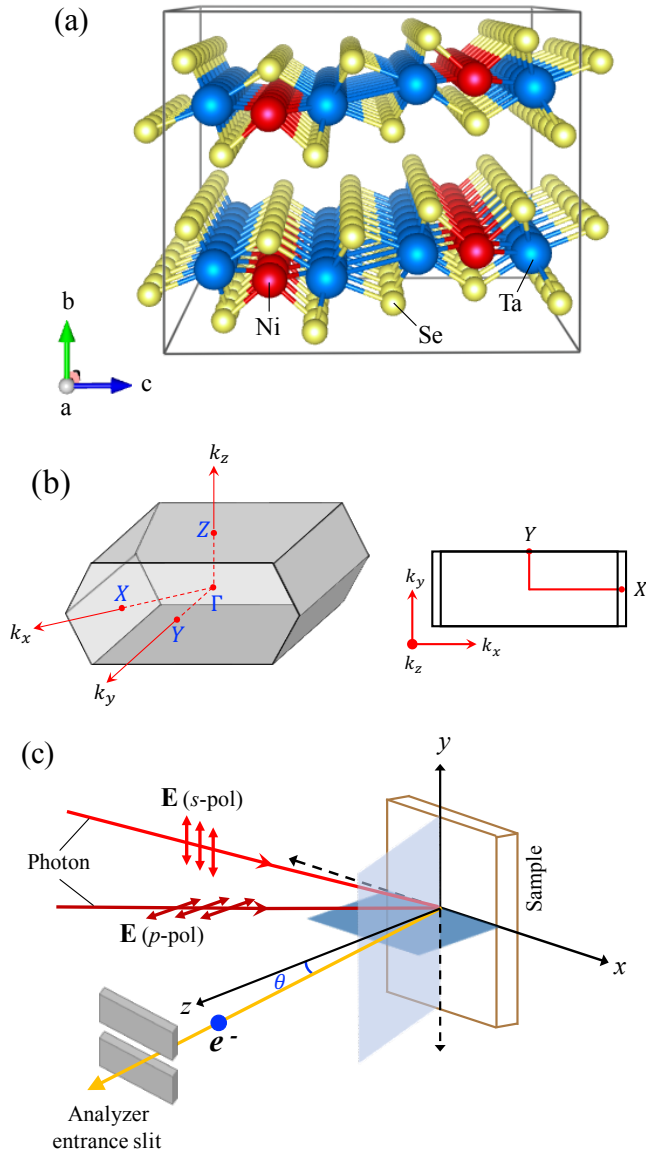


FIG. 1. (a) Crystal structure of Ta₂NiSe₅ in the monoclinic phase where a , b , c define the crystal axis system and tantalum, nickel and selenium atoms are represented by blue, red and yellow spheres, respectively. (b) (left) Bulk Brillouin zone (BZ) of a monoclinic lattice where Γ , X, Y, Z are the high symmetry k -points, (right) Projection of the BZ along k_x - k_y plane. (c) Schematic of the experimental geometry showing the polarization of incident photons with respect to the sample.

perimental technique for probing the occupied energy bands in different solid state materials and can be directly compared to band structure calculations. In the present work, we utilize polarization-dependent ARPES to investigate the effect of increasing Sulfur doping levels on the electronic band structure of Ta₂Ni(Se_{1-x}S_x)₅, notably the changes in E vs. k dispersion of the valence band, along different symmetry directions in k -space. While extensive equilibrium and non-equilibrium studies have been done on pristine Ta₂NiSe₅, the T_c vs. x phase diagram¹⁹ has not been explored through ARPES

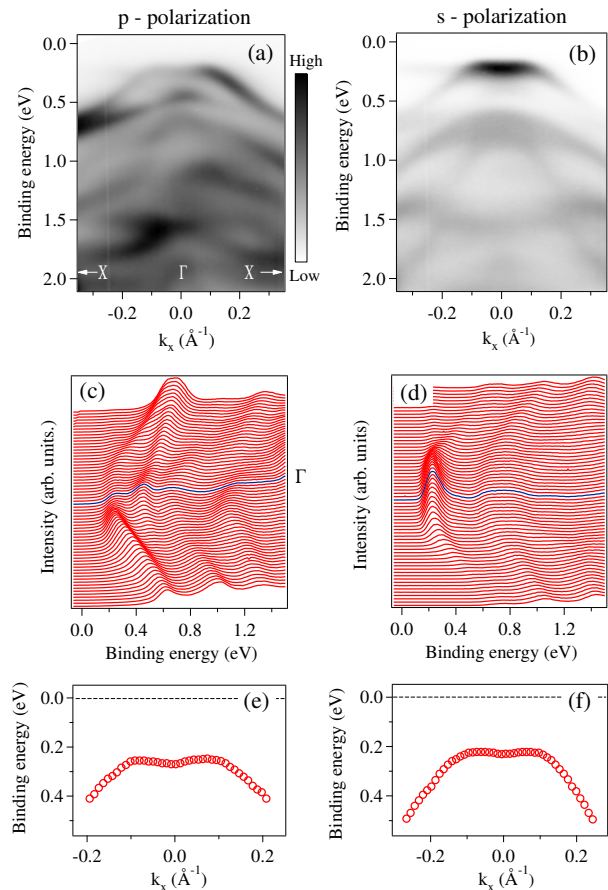


FIG. 2. ARPES intensity maps of Ta₂NiSe₅ along Γ -X direction acquired at $T = 80$ K using (a) p-polarized (horizontal) and (b) s-polarized (vertical) light of photon energy $h\nu = 19$ eV. The extracted energy distribution curves (EDCs) stacked along k_x -axis for p-pol (c) and s-pol (d). The blue curve corresponds to the EDC at Γ ($k_x = 0$) in each case. A zoomed view of the valence band dispersion showing the band flatness near Fermi level, E_F , where the peak positions of the band obtained from the EDCs in (c) and (d) are plotted as a function of k_x for both polarisations, (e) p-pol and (f) s-pol. The dashed line denotes the Fermi level, E_F .

so far. Although the parent compounds are known to possess strongly two-dimensional properties of the electronic structures, which is consistent with the layered structure of Ta₂NiSe₅ and Ta₂NiS₅, our photon-energy dependent ARPES data reveal a possible three dimensionality of the electronic structure in Ta₂Ni(Se_{1-x}S_x)₅ compounds.

II. EXPERIMENTAL DETAILS

Single crystals of Ta₂Ni(Se_{1-x}S_x)₅ (with $x = 0.0$, $x = 0.25$ and $x = 0.50$) were purchased from HQ Graphene (<http://www.hqgraphene.com>). The samples were synthesised by chemical vapour transport (CVT)^{8,40}. The ARPES experiments were carried out at the BaDElPh beamline⁴¹ of the Elettra synchrotron in Trieste, Italy. It offers both horizontal (p-pol) and vertical (s-pol) light

polarizations, a maximum angular resolution of 0.1° and energy resolution of 5.4 meV. A photon energy range from $h\nu = 16$ eV to $h\nu = 34$ eV was used for this study and all the data presented in the paper were acquired at sample temperature $T = 80$ K. Prior to ARPES measurements, clean sample surfaces were obtained via cleaving in the direction perpendicular to the atomic planes. The samples were cleaved under UHV pressure better than 5×10^{-10} mbar and the measurements were performed at a base pressure $< 1 \times 10^{-10}$ mbar.

III. RESULTS AND DISCUSSION

Ta_2NiSe_5 , first reported in Ref.[8], has a layered crystalline structure, where each layer consists of double chains of tantalum (Ta) atoms with single chains of nickel (Ni) atoms in-between. The Ta-Ni-Ta trichains are parallel to the crystallographic a -axis and repeat themselves along the c -axis, exhibiting a quasi-one dimensional structure. Selenium atoms are tetrahedrally and octahedrally coordinated around the Ni atoms and Ta atoms, respectively. The layers are stacked along b -axis and are held together through van der Waals forces. The crystal structure of Ta_2NiSe_5 in its low temperature monoclinic phase is shown in Fig. 1(a). Band structure calculations have shown that the topmost valence band comprises Ni $3d$ and Se $4p$ orbitals while the conduction band bottom is composed of Ta $5d$ orbitals¹¹. The high temperature orthorhombic phase of Ta_2NiSe_5 is characterised by a very small direct band gap while its low temperature monoclinic phase is an excitonic insulator, with a second-order phase transition occurring at $T_c \approx 326$ K²⁸. Excitons are formed by Ni $3d$ - Se $4p$ holes and Ta $5d$ electrons with a flattened dispersion of the valence band top characterising the excitonic insulating state from an ARPES point of view. A schematic of the bulk Brillouin zone of Ta_2NiSe_5 for the monoclinic phase, along with its projection on the $k_x k_y$ plane is shown in Fig. 1(b).

The experimental geometry of the sample plane with respect to the analyser slit and direction of light polarization is schematically represented in Fig. 1(c). Fig. 2 shows an overview of the band structure in Ta_2NiSe_5 for the low temperature phase, revealed by our ARPES measurements along $\Gamma-X$ direction, using light with different linear polarizations. The ARPES spectra in Figs. 2(a)-(b) show that the top part of the valence band centered at Γ ($k_x = 0$) is characterised by a flat band dispersion⁹ which is the signature of an excitonic insulating phase. The stacked energy distribution curves (EDCs) along k_x extracted from the (a)-(b) ARPES intensity plots are shown in Figs 2(c)-(d), respectively, to give a better perspective of the band dispersions, especially the valence band below Fermi level, E_F (referenced to 0). To give a clear picture of the characteristic band flatness close to E_F , the peak energy positions of the topmost valence band determined from the EDCs in (c) and (d) are plotted as a function of k_x in Figs. 2(e) and 2(f), respectively.

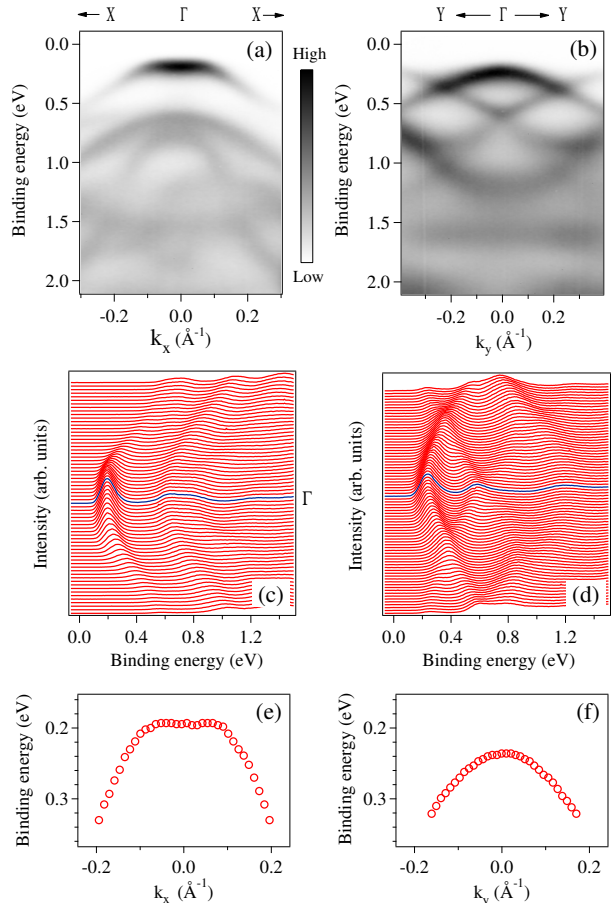


FIG. 3. ARPES intensity maps of 25% S-doped Ta_2NiSe_5 along (a) $\Gamma-X$ and (b) $\Gamma-Y$ directions acquired at $T = 80$ K and photon energy $h\nu = 20$ eV using s -polarized photons. The extracted energy distribution curves (EDCs) stacked along k_x -axis in (c) and k_y -axis in (d). The blue curve corresponds to the EDC at Γ [$k_x = 0$ in (a), $k_y = 0$ in (b)]. A zoomed view of the valence band dispersion near Fermi level, E_F , where the peak positions of the EDCs in (c) and (d) are plotted as a function of k_x and k_y in (e) and (f), respectively.

We observe that the top valence band lies at ~ 0.2 eV below E_F and its dispersion around Γ is hole-like with a flattened top, giving an overall shallow M-shaped dispersion. The parts away from Γ and more towards X are strongly dispersive. A characteristic M-shaped dispersion which becomes sharper on lowering the temperature has been previously reported from ARPES studies done using different light polarization geometries³⁴.

Moving to the polarization dependence of the ARPES spectra, we note from Figs. 2(a) and 2(b) that the photoemission spectra acquired using two different polarization geometries, namely, p-polarization (\mathbf{E} lying in xz plane in Fig. 1(c)) and s-polarization (\mathbf{E} along y -direction in Fig. 1(c)), exhibit strong differences. The spectral weight of the flat top part of the valence band centered at Γ is relatively strong for s-polarization. For the dispersive parts of the valence band which are away from Γ and along the $\Gamma-X$ line, the spectral weight is stronger when probed with p-polarized light. This polarization-

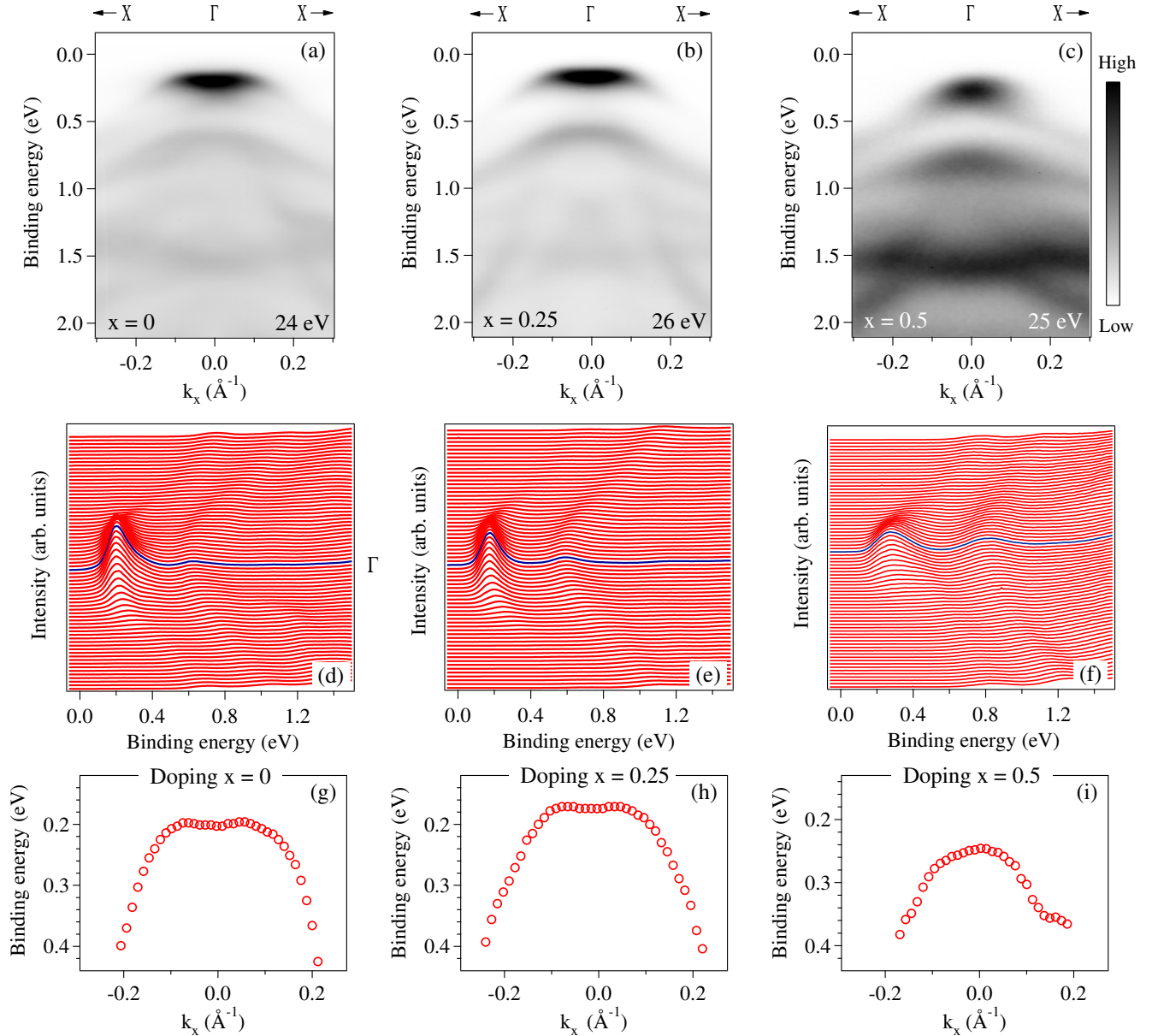


FIG. 4. (a)-(c) ARPES intensity plots of Ta_2NiSe_5 , $\text{Ta}_2\text{Ni}(\text{Se}_{0.75}\text{S}_{0.25})_5$ and $\text{Ta}_2\text{Ni}(\text{Se}_{0.5}\text{S}_{0.5})_5$, respectively, along $\Gamma - X$ direction acquired at photon energies $h\nu = 24$ eV, 26 eV, 25 eV (s-polarization) respectively, and at $T = 80$ K. (d)-(f) Stacked energy distribution curves (EDCs) extracted from their respective ARPES plots in (a)-(c); the blue curve corresponds to the EDC at Γ in each case. (g)-(i) Band dispersion of the top part of the valence band near E_F for $x = 0, 0.25, 0.5$, respectively, obtained from the peak positions of the corresponding EDCs.

dependent contrast continues to exist at different photon energies explored and hence is attributed to the symmetry selection rules of the photoemission process^{42,43}. Similar symmetry contrasts are also observed in 25% and 50% S-doped Ta_2NiSe_5 (Supplementary Material, Section A). Such drastic changes in the spectral intensity of polarization-dependent ARPES data can help us identify the mirror symmetries associated with different atomic orbitals. From now on, we will only show the data acquired using s-polarized light due to the better visibility of the top part of the valence band, which is relevant for the excitonic insulator phase.

Although Ta_2NiSe_5 is believed to form a quasi-one-

dimensional structure, the hopping of mobile carriers along c -axis gives rise to a two-dimensional (2D) character of the electronic band structure. There exists an anisotropy in the band dispersions of Ta_2NiSe_5 ^{34,44,45} and Ta_2NiS_5 ¹² along $\Gamma - X$ and $\Gamma - Y$ directions. Our ARPES data reveal similar anisotropic properties of the electronic structure in Sulfur-doped Ta_2NiSe_5 as well. The ARPES intensity maps along $\Gamma - X$ and $\Gamma - Y$ (refer to Fig. 1(b) for the k -space symmetry points) of $\text{Ta}_2\text{Ni}(\text{Se}_{1-x}\text{S}_x)_5$ for $x = 0.25$ are shown in Figs. 3(a) and 3(b), respectively. We observe that the dispersion around Γ point along k_x -axis ($\Gamma - X$ direction) is characterised by a flat feature of the valence band top while the

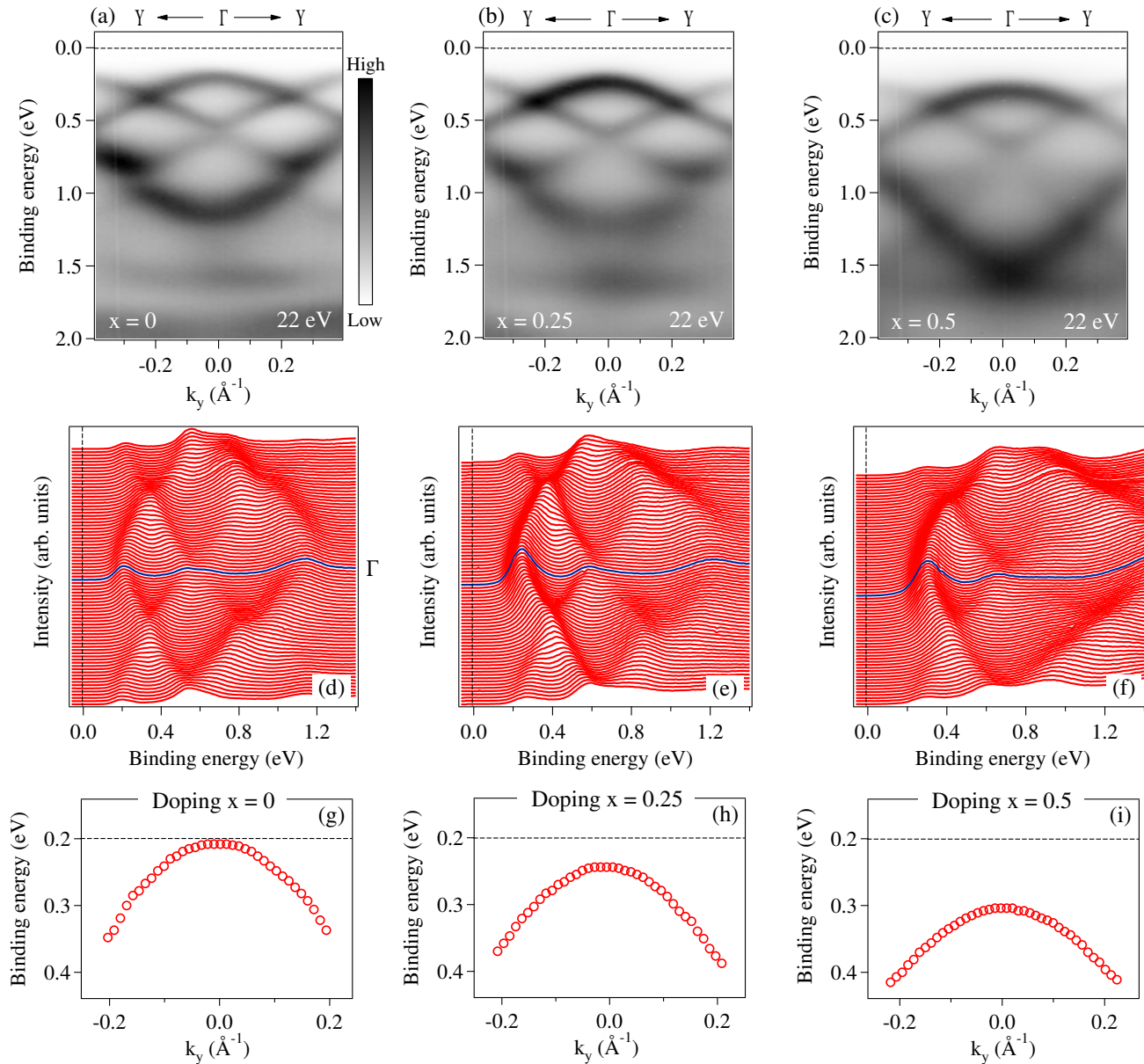


FIG. 5. (a)-(c) ARPES intensity plots of Ta_2NiSe_5 , $\text{Ta}_2\text{Ni}(\text{Se}_{0.75}\text{S}_{0.25})_5$ and $\text{Ta}_2\text{Ni}(\text{Se}_{0.5}\text{S}_{0.5})_5$, respectively, along $\Gamma - Y$ direction acquired at photon energy $h\nu = 22$ eV (s-polarization) and at $T = 80$ K. (d)-(f) Stacked energy distribution curves (EDCs) extracted from their respective ARPES plots in (a)-(c); the blue curve corresponds to the EDC at Γ in each case. The dashed lines in (a)-(f) denote the Fermi level, E_F . (g)-(i) Band dispersion of the top part of the valence band near E_F for $x = 0, 0.25, 0.5$ respectively obtained from the peak position of the corresponding EDCs. The dashed line denotes the peak position at Γ for $x = 0$.

dispersion of the valence band at Γ along k_y -axis ($\Gamma - Y$ direction) does not exhibit the hybridized flattened band dispersion. The periodicity of the band dispersion along k_y in 3(b) could be easily captured with the photon energy range used in this study, due to its small periodicity along $\Gamma - Y$ direction. For better clarity of the band dispersions along both directions, the corresponding stacked EDC plots are displayed in Figs. 3(c) and 3(d). A zoomed view of the dispersion for the top part of the valence band centered at Γ along k_x and k_y directions is presented in Figs. 3(e) and 3(f), respectively. The dispersions have been obtained from the peak energy

positions of the corresponding EDCs (3(c) and 3(d)) for the valence band top below E_F . The flat band feature around Γ along k_x is clearly seen while the dispersion of the valence band top along k_y seems to be parabolic. For completeness, the anisotropic dispersions for pristine Ta_2NiSe_5 and $\text{Ta}_2\text{Ni}(\text{Se}_{1-x}\text{S}_x)_5$ ($x = 0.5$) are presented in the Supplementary Material (Section B). Because the bands also show a dispersion in the (in-plane) direction perpendicular to the chains, the quasi-1D structure often assumed for this family of compounds does not fully describe the electronic structure in these materials.

We now study the effect of Sulphur doping on the

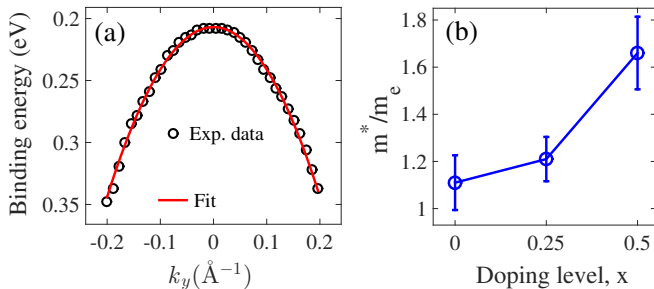


FIG. 6. (a) Fit (red curve) to the E vs. k dispersion (black circles) around Γ in pristine Ta_2NiSe_5 . (b) Effective mass m^* (in units of electron rest mass, m_e) at different doping levels, x .

electronic structure of Ta_2NiSe_5 , i.e., the band dispersions in $\text{Ta}_2\text{Ni}(\text{Se}_{1-x}\text{S}_x)_5$, with increasing values of x . Fig. 4 shows the evolution of the band dispersion along $\Gamma-X$ direction in $\text{Ta}_2\text{Ni}(\text{Se}_{1-x}\text{S}_x)_5$ with x changing from 0 to 0.5. We observe that for Sulfur doping levels of $x = 0, 0.25$ and 0.5 , the band structure retains the main dispersive features down to approximately 2 eV below E_F , except for the top-part of the valence band at Γ . The relative changes in intensity are due to different photoionization cross sections at different photon energies. What is interesting to note here is that while the band flatness with the shallow M-shape is present for pristine Ta_2NiSe_5 (0% S-doping in Figs. 4(a), (d)) and remains unaffected under 25% Sulfur doping (see Figs. 4(b), (e)), it is significantly distorted for a substantial S-doping level of 50% (see Figs. 4(c), (f)). Since the flattened dispersion of the valence band top is a fingerprint of the excitonic insulator phase, the observed deviation is indicative of the suppression of an excitonic insulator phase under heavy S-doping. For better clarity, the valence band dispersions around Γ extracted from their respective EDC plots are displayed in Figs. 4(g)–(i). The flat band distortion can be understood considering the size of the band gap E_g in the high temperature phase of $\text{Ta}_2\text{Ni}(\text{Se}_{1-x}\text{S}_x)_5$. Indeed, with increasing levels of Sulfur doping, the band gap E_g monotonically increases, thereby, suppressing the spontaneous formation of excitons. Hence, the excitonic insulating state becomes unstable against the semiconducting ground state. This emphasizes that although an excitonic insulator phase in Ta_2NiSe_5 can be realized with 25% of S-doping at 80 K, the excitonic ground state is destroyed when the doping level is $\approx 50\%$. Electrical transport studies have revealed that a similar S-doping level (i.e., $x \geq 0.5$) does not allow to observe the excitonic phase transition, down to 2K.

We now turn to the evolution of the band structure along $\Gamma-Y$ direction as a function of S-doping. Figs. 5(a)–(c) shows the band structure of $\text{Ta}_2\text{Ni}(\text{Se}_{1-x}\text{S}_x)_5$ for $x = 0, 0.25, 0.5$ and the corresponding stacked EDCs are plotted in Figs. 5(d)–(f) for better visualization of the band dispersions. As already shown in Figs. 3(b), (d) and (f), the valence band near E_F is characterised by a hole-like parabolic dispersion along k_y centred at Γ -point. From the ARPES intensity maps [Figs. 5(a)–(c)], we see that the band dispersions along k_y -direction have subtle changes in the binding

energies of different states for 25% S-doping [Fig. 5(e)] but pronounced changes for 50% S-doping [Fig. 5(f)], when compared to the energy states in pristine Ta_2NiSe_5 [Fig. 5(d)]. The dispersion of the valence band around Γ near E_F for the three doping levels are compared in Figs. 5(g)–(i). We notice that by increasing the amount of S-doping, the parabolic dispersion centered at Γ shifts to higher binding energies resulting in an overall enhancement of the energy gap along $\Gamma-Y$ direction. As stated before, the valence band is composed of Ni 3d and Se 4p (S 3p) orbitals. Therefore, increasing substitution by Sulfur atoms at the Se atom sites brings the states at the top of the valence band to higher binding energies. Another interesting fact that can be noted from the band dispersions is the change in effective mass ratio, m^*/m_e (where, m_e is the rest mass of an electron), in $\text{Ta}_2\text{Ni}(\text{Se}_{1-x}\text{S}_x)_5$ at different S-doping levels. The valence band dispersions along $\Gamma-Y$ have been fitted with quadratic functions, $E_0 - \hbar^2 k^2 / 2m^*$ (\hbar is the Planck's constant), with two fitting parameters E_0 and m^* . The experimental data in Figs. 5(g)–(i) are well reproduced by the fits, an example of which is shown in Fig. 6(a). The values of m^* obtained from the fits are plotted in units of m_e as a function of S-doping level in Fig. 6(b). We observe that while there is a small difference in the values of m^*/m_e between $x = 0$ and $x = 0.25$, it is comparatively larger for $x = 0.5$. This is expected due to stronger carrier localization with increasing S-doping levels which arises from hybridized Ni 3d and S 3p orbitals, leading to higher effective masses. Such a result is consistent with our observations in Figs. 5(g)–(i), where the energy states move towards higher binding energies as S-doping is increased.

Next, we investigate whether the band dispersion in $\text{Ta}_2\text{Ni}(\text{Se}_{1-x}\text{S}_x)_5$ exhibits a three-dimensional character. The three dimensionality of the electronic structure can be determined by probing the out-of-plane $\Gamma-Z$ direction which corresponds to k_\perp in our experimental geometry. A photon energy dependent ARPES study is required to obtain such an information. Figures 7(a)–(e) shows the E vs. k maps of $\text{Ta}_2\text{Ni}(\text{Se}_{1-x}\text{S}_x)_5$, $x = 0.25$, along $\Gamma-X$ direction acquired at different photon energies. Due to low photoionization cross section at photon energies below 15 eV and above 35 eV, a photon energy range from 16 eV to 34 eV was chosen. Looking at ARPES intensity maps, one can notice a photon energy-dependent cross sectional contrast, as well as a considerable variation of the binding energies of different bands, especially for bands lying between 0.5 eV and 1 eV below E_F and the flat band near E_F . We will mainly concentrate on the energy modifications of the ‘flat band’ with variations in photon energy. The EDCs at Γ -point [along the red dotted line in Fig. 7(a)] within 0.3 eV below E_F , capturing only the spectral intensity of the flat band, are plotted for different photon energies in Fig. 7(f). From the ARPES images and the EDC plots, the obvious trend that we observe is the shift of the flat band towards E_F on increasing the photon energy. This is clearly seen if one notes the energy separation between 0 eV binding energy (or E_F , shown by black dashed line) and the flat

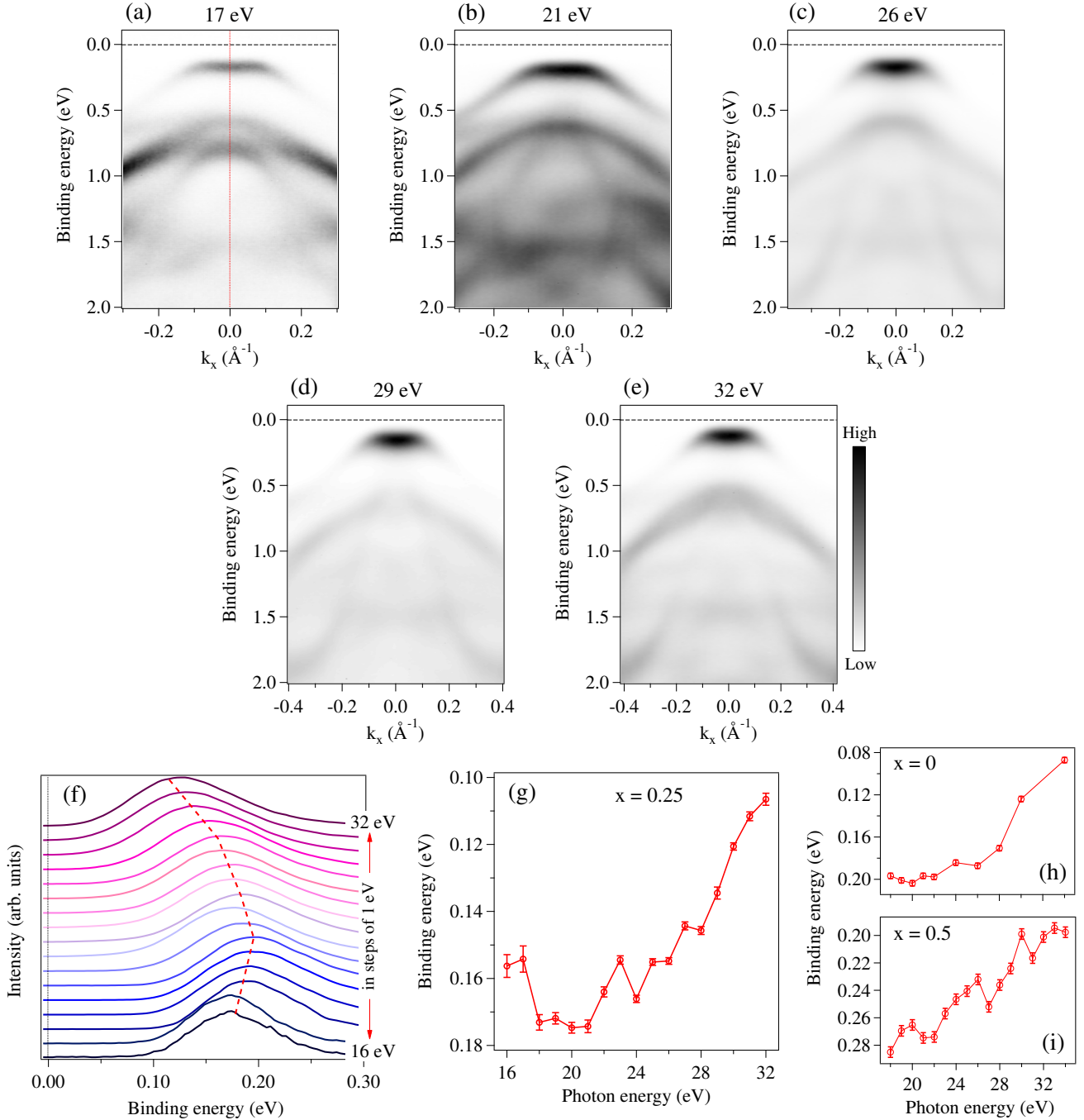


FIG. 7. (a)-(e) ARPES intensity plots of $\text{Ta}_2\text{Ni}(\text{Se}_{0.75}\text{S}_{0.25})_5$ ($T = 80$ K) along $\Gamma - X$ direction for s-polarized light at photon energies, $h\nu = 17$ eV, 21 eV, 26 eV, 29 eV, 32 eV respectively. The Γ -point is denoted by the red dotted line in (a) and the dashed lines in (a)-(e) at 0 eV binding energy denote E_F . (f) EDCs at Γ for different photon energies covering a range from $h\nu = 16$ eV to 32 eV with a step size of 1 eV. The red dashed line is a guide to the eye following the peak position of the valence band with increasing photon energy. (g) Peak position of the valence band obtained by fitting the EDCs with a Lorentzian-Gaussian line shape at Γ as a function of photon energy. (h), (i) Dependence of the valence band peak position on photon energy in pristine and 50% S-doped Ta_2NiSe_5 , respectively.

band below it in Figs. 7(a)-(e). The dispersion of the flat band along k_{\perp} can be visualized from the red dashed line denoting the peak position of the EDCs at different photon energies in Fig. 7(f). The peak position of the flat band relative to E_F at different photon energies has been obtained by fitting each of the EDCs with a

Gaussian-Lorentzian distribution function after Shirley background subtraction. Fig. 7(g) shows that the peak position of the flat band at Γ moves towards E_F with increasing photon energy, with a dip at $h\nu \approx 20$ eV. A decrease in the binding energy of the flat band in Ta_2NiSe_5 and the distorted flat band in $\text{Ta}_2\text{Ni}(\text{Se}_{0.5}\text{S}_{0.5})_5$ at Γ -

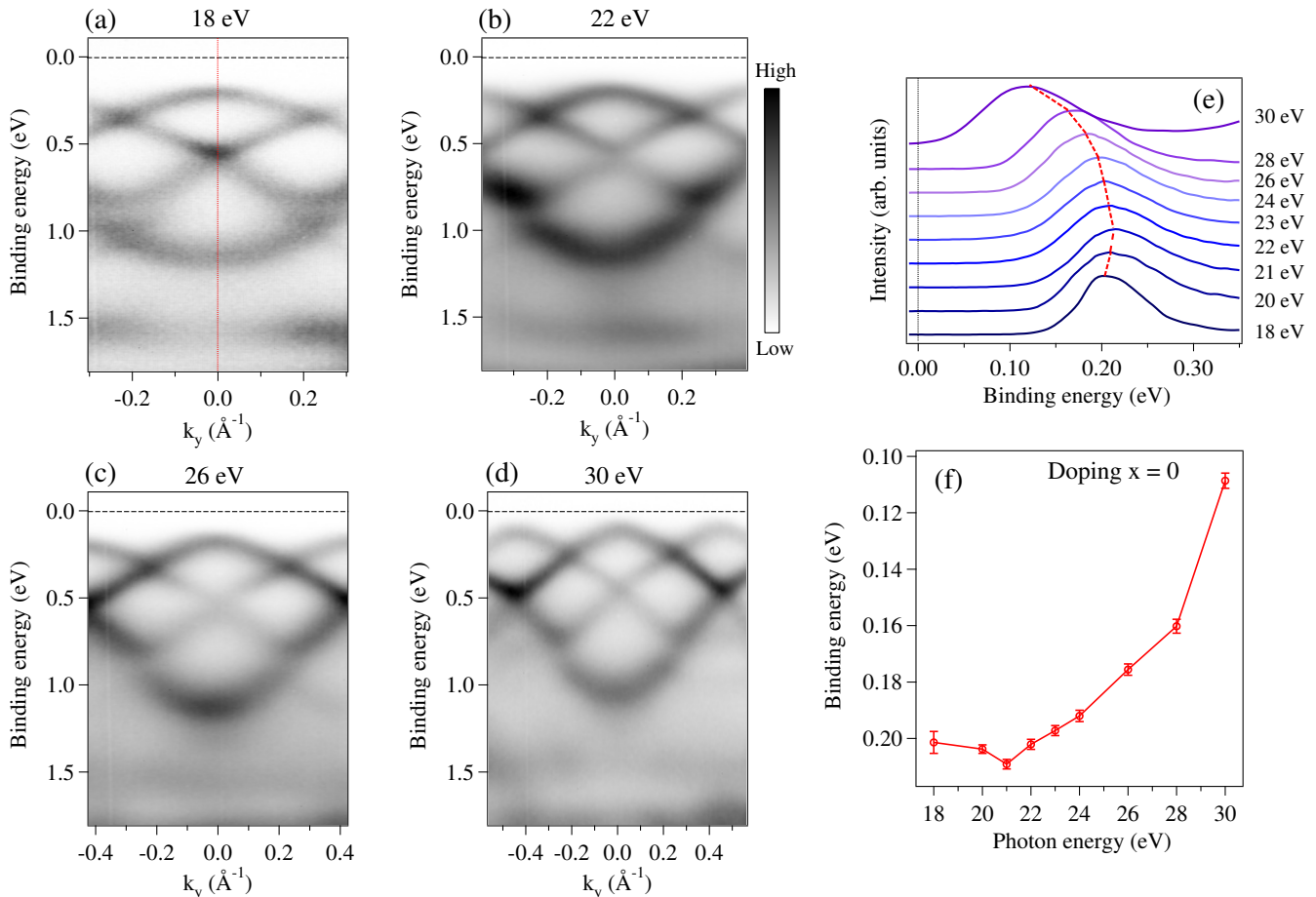


FIG. 8. (a)-(d) ARPES intensity plots of pristine Ta_2NiSe_5 ($T = 80$ K) along $\Gamma - Y$ direction for s-polarized light at photon energies, $h\nu = 18$ eV, 22 eV, 26 eV, 30 eV respectively. The Γ -point is denoted by the red dotted line in (a) and the dashed lines in (a)-(d) at 0 eV binding energy denote E_F . (e) EDCs at Γ for various photon energies. The red dashed line is a guide to the eye following the peak position of the valence band with increasing photon energy. (f) Peak position of the valence band obtained by fitting the EDCs at Γ as a function of photon energy.

point ($\Gamma - X$ direction) with increasing photon energy are shown in Figs. 7(h) and (i), respectively. There are no pronounced qualitative differences in the trend of binding energy vs photon energy curves amongst the three compounds (Supplementary Material, Section C). For a perfectly two-dimensional electronic structure often used for Ta_2NiSe_5 and Ta_2NiS_5 , the band dispersions should be independent of k_z (k_\perp in our experimental geometry) but the above observations clearly show a dispersion along k_z , i.e., along $\Gamma - Z$ direction in Fig. 1(b). This demonstrates the three-dimensionality of electronic band structure in this family of compounds.

For completeness, we also present the photon energy dependence of the band structure along $\Gamma - Y$ direction. Figs. 8(a)-(d) show the ARPES intensity plots at different photon energies for pristine Ta_2NiSe_5 . Again, an overall energy shift of the band structure towards E_F (denoted by black dashed lines in the 2D-plots) is observed with increasing photon energies. The EDCs containing only the top-part of the valence band at Γ are plotted for various photon energies in Fig. 8(e). A similar trend in the shift of valence band peak position as

that in Fig. 7(f) can be noted here (marked by the red dashed line). The photon energy-dependent peak positions are plotted in Fig. 8(f), where a decrease in binding energy is observed, thereby demonstrating a clear dispersion along $\Gamma - Z$ direction. The above results of the photon energy dependent ARPES measurements in all the three compounds do emphasize that inspite of the well known layered structure characterizing the $\text{Ta}_2\text{Ni}(\text{Se}_{1-x}\text{S}_x)_5$ compounds, the electronic structure is not strictly two-dimensional.

IV. CONCLUSION

To summarize, we investigated the evolution of the band structure in $\text{Ta}_2\text{Ni}(\text{Se}_{1-x}\text{S}_x)_5$, as a function of Sulfur concentration x and its three-dimensionality using ARPES. The anisotropy of the in-plane band dispersions along $\Gamma - X$ and $\Gamma - Y$ directions in the doped compounds is clearly revealed. A substantial amount of Sulfur doping $\sim 50\%$ is able to suppress the excitonic ground state in $\text{Ta}_2\text{Ni}(\text{Se}_{1-x}\text{S}_x)_5$. This can be claimed due to

the observed deviation of the dispersion of valence band top from its flattened E vs. k feature along $\Gamma - X$ at $x = 0.5$ but not at $x = 0.25$. The suppression of the excitonic insulator state is followed by a pronounced increase in the effective mass m^* for the highest doping level, indicating stronger localization of the charge carriers, which is in agreement with the weakening of hybridization between Ni $3d$ and Se $4p$ (S $3p$) orbitals that also leads to larger values of E_g . Our photon-energy dependent ARPES data show a gradual decrease in the binding energy of states near Fermi level on increasing the photon energy (increasing k_z). This emphasizes that the two-dimensional picture often used for Ta_2NiSe_5 (and Ta_2NiS_5 , not studied in this work) does not fully represent the entire electronic structure and that three-dimensionality must be taken into account when studying $\text{Ta}_2\text{Ni}(\text{Se}_{1-x}\text{S}_x)_5$ compounds. Dimensionality of the underlying electronic structure in a material is an important parameter while choosing potential candidates for electronic applications. Low-dimensional systems have sur-

passed their bulk counterparts in this field due to their high electrical and thermal conductivities. Our results therefore suggest that the three-dimensional nature of $\text{Ta}_2\text{Ni}(\text{Se}_{1-x}\text{S}_x)_5$ needs to be taken into account when considering these compounds for applications in the field of electronics and optoelectronics.

ACKNOWLEDGMENTS

This project has received funding from the European Union's Horizon 2020 research and innovation programme under grant agreement No 654360 NFFA-Europe. The authors acknowledge Elettra Sincrotrone Trieste for providing access to its synchrotron radiation facilities and to the BaDELPH beamline that contributed to the results presented in this work. We thank L. Sancin for technical assistance during experiments and J. Mravlje and F. Galdenzi for fruitful discussions during the beamtime.

-
- * Corresponding author: tanusree.saha@student.ung.si
- ¹ B. W. H. Baugher, H. O. H. Churchill, Y. Yang, and P. J.-Herrero, *Nano Lett.* **13**, 4212 (2013).
 - ² X. Cui, G.-H. Lee, Y. D. Kim, G. Arefe, P. Y. Huang, C.-H. Lee, D. A. Chenet, X. Zhang, L. Wang, F. Ye, F. Pizzocchero, B. S. Jessen, K. Watanabe, T. Taniguchi, D. A. Muller, T. Low, P. Kim and J. Hone, *Nature Nanotechnology* **10**, 534 (2015).
 - ³ J. L. Webb, L. S. Hart, D. Wolverson, C. Chen, J. Avila, and M. C. Asensio, *Phys. Rev. B* **96**, 115205 (2017).
 - ⁴ J. N. Coleman *et al.*, *Science* **331**, 568 (2011).
 - ⁵ T. I. Larkin, A. N. Yaresko, D. Pröpper, K. A. Kikoin, Y. F. Lu, T. Takayama, Y.-L. Mathis, A. W. Rost, H. Takagi, B. Keimer, and A. V. Boris, *Phys. Rev. B* **95**, 195144 (2017).
 - ⁶ L. Li, P. Gong, W. Wang, B. Deng, L. Pi, J. Yu, X. Zhou, X. Shi, H. L. Orcid and T. Zhai, *ACS Nano* **11**, 10264 (2017).
 - ⁷ S. Y. Kim, Y. Kim, C.-J. Kang, E.-S. An, H. K. Kim, M. J. Eom, M. Lee, C. Park, T.-H. Kim, H. C. Choi, B. I. Min and J. S. Kim, *ACS Nano* **10**, 8888 (2016).
 - ⁸ S. A. Sunshine and J. A. Ibers, *Inorg. Chem.*, **24**, 3611 (1985).
 - ⁹ Y. Wakisaka, T. Sudayama, K. Takudo, T. Mizokawa, M. Arita, H. Namatame, M. Taniguchi, N. Katayama, M. Nohara and H. Takagi, *Phys. Rev. Lett.* **103**, 026402 (2009).
 - ¹⁰ K. Seki, Y. Wakisaka, T. Kaneko, T. Toriyama, T. Konishi, T. Sudayama, N. L. Saini, M. Arita, H. Namatame, M. Taniguchi, N. Katayama, M. Nohara, H. Takagi, T. Mizokawa and Y. Ohta, *Phys. Rev. B* **90**, 155116 (2014).
 - ¹¹ T. Kaneko, T. Toriyama, T. Konishi and Y. Ohta, *Phys. Rev. B* **87**, 035121 (2013).
 - ¹² K. Mu, H. Chen, Y. Li, Y. Zhang, P. Wang, B. Zhang, Y. Liu, G. Zhang, L. Song and Z. Sun, *J. Mater. Chem. C* **6**, 3976 (2018).
 - ¹³ R. Knox, *Theory of Excitons* (Academic, New York, 1963).
 - ¹⁴ N. F. Mott, *Philos. Mag.* **6**, 287 (1961).
 - ¹⁵ B. I. Halperin and T. M. Rice, *Rev. Mod. Phys.* **40**, 755 (1968).
 - ¹⁶ W. Kohn, *Phys. Rev. Lett.* **19**, 439 (1967).
 - ¹⁷ D. Jérôme, T. M. Rice and W. Kohn, *Phys. Rev.* **158**, 462 (1967).
 - ¹⁸ K. Matsubayashi, *CiNii Articles*. Available at <http://ci.nii.ac.jp/naid/110009990261/en> (2015).
 - ¹⁹ Y. F. Lu, H. Kono, T. I. Larkin, A. W. Rost, T. Takayama, A. V. Boris, B. Keimer and H. Takagi, *Nat. Commun.* **8**, 14408 (2017).
 - ²⁰ J. A. Wilson, *Solid State Commun.* **22**, 551 (1977).
 - ²¹ H. Cercellier, C. Monney, F. Clerc, C. Battaglia, L. Despont, M. G. Garnier, H. Beck, P. Aebi, L. Patthey, H. Berger, and L. Forró, *Phys. Rev. Lett.* **99**, 146403 (2007).
 - ²² B. Bucher, P. Steiner, and P. Wachter, *Phys. Rev. Lett.* **67**, 2717 (1991).
 - ²³ L. Du, X. Li, W. Lou, G. Sullivan, K. Chang, J. Kono and R. R. Du, *Nat. Commun.* **8**, 1971 (2017).
 - ²⁴ R. A. Craven, F. J. Di Salvo and F. S. L. Hsu, *Solid State Commun.* **25**, 39 (1978).
 - ²⁵ B. Bucher, T. Park, J. D. Thompson and P. Wachter, Preprint at <https://arxiv.org/abs/0802.3354> (2008).
 - ²⁶ H. P. Hughes, *J. Phys. C: Solid State Phys.* **10**, L319 (1977).
 - ²⁷ J. Ishioka, Y. H. Liu, K. Shimatake, T. Kurosawa, K. Ichimura, Y. Toda, M. Oda, and S. Tanda, *Phys. Rev. Lett.* **105**, 176401 (2010).
 - ²⁸ F. J. Di Salvo, C. H. Chen, R. M. Fleming, J. V. Waszczak, R. G. Dunn, S. A. Sunshine and J. A. Ibers, *J. Less Common Metals* **116**, 51 (1986).
 - ²⁹ D. Golež, P. Werner and M. Eckstein, *Phys. Rev. B* **94**, 035121 (2016).
 - ³⁰ M. Babadi, E. Demler and M. Knap, *Phys. Rev. X* **5**, 041005 (2015).
 - ³¹ M. Babadi, M. Knap, I. Martin, G. Refael and E. Demler, *Phys. Rev. B* **96**, 014512 (2017).
 - ³² K. Kim, H. Kim, J. Kim, C. Kwon, J. S. Kim, and B. J. Kim, *Nature Commun.* **12**, 1969 (2021).
 - ³³ T. I. Larkin, R. D. Dawson, M. Höppner, T. Takayama, M. Isobe, Y.-L. Mathis, H. Takagi, B. Keimer, and A. V. Boris, *Phys. Rev. B* **98**, 125113 (2018).

- ³⁴ M. D. Watson, I. Marković, E. A. Morales, P. Le Fèvre, M. Merz, A. A. Haghighirad and P. D. C. King, *Phys. Rev. Research* **2**, 013236 (2020).
- ³⁵ S. Mor, M. Herzog, D. Golež, P. Werner, M. Eckstein, N. Katayama, M. Nohara, H. Takagi, T. Mizokawa, C. Monney, and J. Stähler, *Phys. Rev. Lett.* **119**, 086401 (2017).
- ³⁶ E. Baldini, A. Zong, D. Choi, C. Lee, M. H. Michael, L. Windgatter, I. I. Mazin, S. Latini, D. Azoury, B. Lv, A. Kogar, Y. Wang, Y. Lu, T. Takayama, H. Takagi, A. J. Millis, A. Rubio, E. Demler and N. Gedik, arXiv:2007.02909.
- ³⁷ T. Saha, D. Golež, G. D. Ninno, J. Mravlje, Y. Murakami, B. Ressel, M. Stupar and P. R. Ribič, *Phys. Rev. B* **103**, 144304 (2021).
- ³⁸ T. I. Larkin, *Online Publikationen der Universität Stuttgart*. Available at <http://dx.doi.org/10.18419/opus-8843> (2016).
- ³⁹ S. Hüfner, *Photoelectron spectroscopy (principles and applications)* Springer series in solid-state sciences (1995).
- ⁴⁰ For a review of transport reactions see: Harald Schafer, "Chemical Transport Reactions". Academic Press, New York, (1964).
- ⁴¹ L. Petaccia, P. Vilmercati, S. Gorovikov, M. Barnaba, A. Bianco, D. Cocco, C. Masciovecchio and A. Goldoni, *Nuclear Instruments and Methods in Physics Research A* **606**, 780 (2009).
- ⁴² J. Harmanson, *Solid State Commun.* **22**, 9 (1977).
- ⁴³ A. Damascelli, Z. Hussain and Z. X. Shen, *Rev. Mod. Phys.* **75**, 473 (2003).
- ⁴⁴ K. Fukutani, R. Stania, C. H. Kwon, J. S. Kim, K. J. Kong, J. Kim and H. W. Yeom, *Nature Physics* **17**, 1024 (2021).
- ⁴⁵ Y. Wakisaka, T. Sudayama, K. Takubo, T. Mizokawa, N. L. Saini, M. Arita, H. Namatame, M. Taniguchi, N. Katayama, M. Nohara and H. Takagi, *J. Supercond. Novel Magn.* **25**, 1231 (2012).

Supplementary Material for:
Electronic band structure in pristine and Sulfur-doped Ta₂NiSe₅

Tanusree Saha,^{1,*} Luca Petaccia,² Barbara Ressel,¹ Primož Rebernik
Ribič,² Giovanni Di Santo,² Wenjuan Zhao,² and Giovanni De Ninno^{1,2}

¹*Laboratory of Quantum Optics, University of Nova Gorica, 5001 Nova Gorica, Slovenia.*

²*Elettra Sincrotrone Trieste, Strada Statale 14 km 163.5, 34149 Trieste, Italy*

(Dated: June 1, 2022)

CONTENTS

A. Polarization dependent ARPES data in $\text{Ta}_2\text{Ni}(\text{Se}_{0.75}\text{S}_{0.25})_5$ and $\text{Ta}_2\text{Ni}(\text{Se}_{0.5}\text{S}_{0.5})_5$	3
B. Anisotropic in-plane band dispersions in Ta_2NiSe_5 and $\text{Ta}_2\text{Ni}(\text{Se}_{0.5}\text{S}_{0.5})_5$	4
C. Comparison of photon energy dependence of valence band peak position among $\text{Ta}_2\text{Ni}(\text{Se}_{1-x}\text{S}_x)_5$ compounds	5
References	5

A. Polarization dependent ARPES data in $\text{Ta}_2\text{Ni}(\text{Se}_{0.75}\text{S}_{0.25})_5$ and $\text{Ta}_2\text{Ni}(\text{Se}_{0.5}\text{S}_{0.5})_5$

Fig. S1 shows the ARPES intensity plots of 25% and 50% Sulphur-doped Ta_2NiSe_5 acquired using xz (p) and y (s) - polarized light. The intensity of the top part of the valence band around Γ is enhanced for s-polarization [see Fig. S1(b) and (d)] while the dispersive parts of the valence band away from Γ (and towards X) display higher intensities for p-polarized light [see Fig. S1(a) and (c)]. This reveals the mirror symmetries associated with different orbitals forming the valence band in these compounds with respect to the xz plane (for our experimental setup).

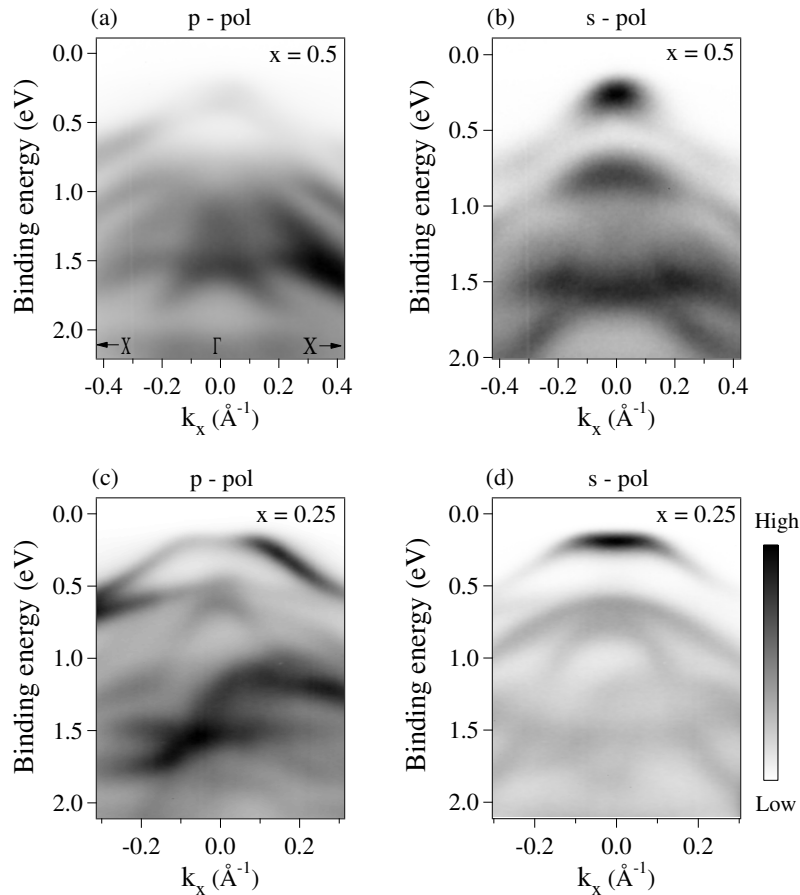


FIG. S1. ARPES intensity maps of $\text{Ta}_2\text{Ni}(\text{Se}_{0.5}\text{S}_{0.5})_5$ acquired along $\Gamma - X$ direction at $T = 80$ K and at photon energy 26 eV using (a) p-polarized light and (b) s-polarized light. The same for $\text{Ta}_2\text{Ni}(\text{Se}_{0.75}\text{S}_{0.25})_5$ in (c) and (d), respectively at photon energy 20 eV.

B. Anisotropic in-plane band dispersions in Ta_2NiSe_5 and $\text{Ta}_2\text{Ni}(\text{Se}_{0.5}\text{S}_{0.5})_5$

The in-plane anisotropy of the energy band dispersions along $\Gamma - X$ and $\Gamma - Y$ directions for Ta_2NiSe_5 having 0% and 50% of Sulphur-doping is shown in Fig. S2(a), (b) and Fig. S2(c), (d), respectively. The valence band near the Fermi level, E_F , exhibits a hole-like dispersion centered at Γ and is characterized by a stronger dispersion along $\Gamma - X$ direction (parallel to the Ta-Ni-Ta chains) than along $\Gamma - Y$ direction (perpendicular to the chains). This indicates that the hopping properties of the carriers are different along the a -axis and c -axis.

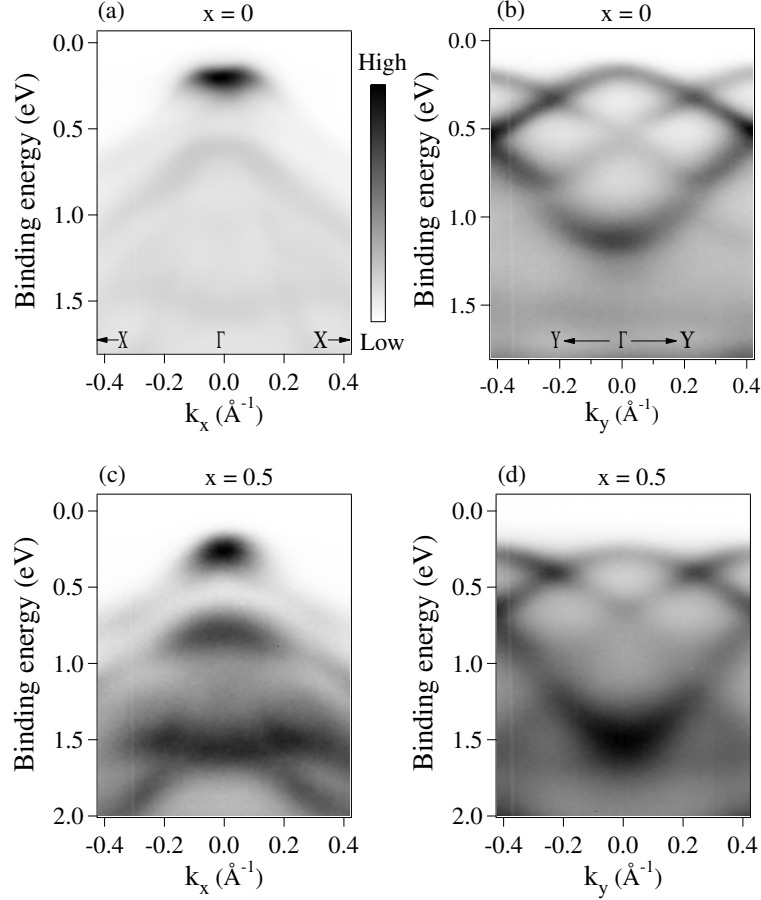


FIG. S2. (a) and (b) Anisotropic band dispersions along $\Gamma - X$ and $\Gamma - Y$ directions in Ta_2NiSe_5 . Band dispersions along $\Gamma - X$ and $\Gamma - Y$ in $\text{Ta}_2\text{Ni}(\text{Se}_{0.5}\text{S}_{0.5})_5$ in (c) and (d), respectively. A photon energy of 26 eV and s-polarized light is used.

C. Comparison of photon energy dependence of valence band peak position among $\text{Ta}_2\text{Ni}(\text{Se}_{1-x}\text{S}_x)_5$ compounds

Fig. S3 shows a comparison of the valence band peak position at Γ along $\Gamma - X$ direction as a function of the incident photon energy for the three doped (0%, 25%, 50%) compounds. The binding energy values have been plotted on the $(E_b - E_{b,\min})/(E_{b,\max} - E_{b,\min})$ scale for each of the compounds. Apart from the quantitative differences in the binding energy, E_b , values between the three curves (red, black, blue in Fig. S3), the overall trend, i.e., a decrease in the binding energy with increasing photon energy, does not show any pronounced qualitative differences between the three compounds, at least within the photon energy range used for this study.

All the data analysis has been performed using Igor Pro (wavemetrics.com) and Casa XPS (<http://www.casaxps.com>) softwares and the crystal structure in Fig. 1(a) was generated in VESTA¹.

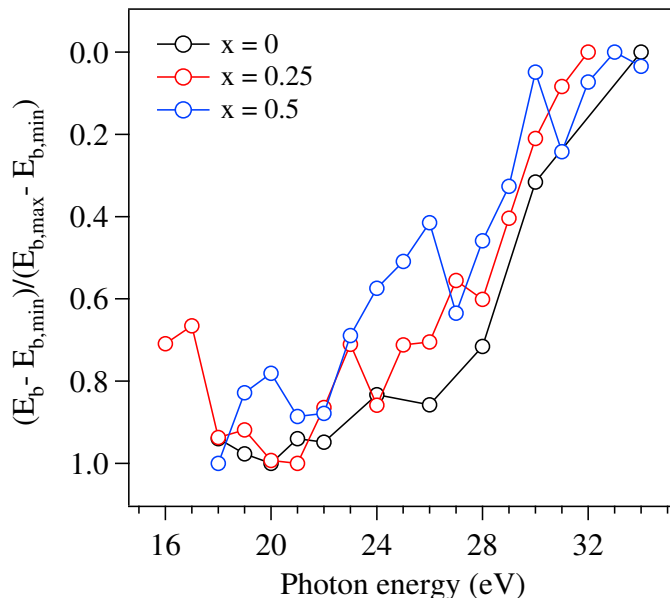


FIG. S3. Peak position of the valence band at Γ [shown in Fig.7(g)-(i)] as a function of incident photon energy for pure and S-doped Ta_2NiSe_5 , plotted on the same relative scale for comparison. E_b stands for the binding energy.

* Corresponding author: tanusree.saha@student.ung.si

¹ K. Momma and F. Izumi, J. Appl. Crystallogr. **44**, 1272 (2011).